

Determination of the Transport and Optical Properties of a Nonideal Solid Plasma Produced by Femtosecond Laser Pulses

M. B. Agranat, N. E. Andreev, S. I. Ashitkov, M. E. Veisman, P. R. Levashov, A. V. Ovchinnikov, D. S. Sitnikov, V. E. Fortov, and K. V. Khishchenko

Institute of High Energy Densities, Russian Academy of Sciences, ul. Izhorskaya 13/19, Moscow, 125412 Russia

Received November 28, 2006; in final form, February 12, 2007

Experimental data on the amplitude and phase of the complex reflection coefficient of a laser pulse from a nonideal solid plasma, which is produced on the surface of a metallic target by intense femtosecond laser radiation, have been obtained using femtosecond interference microscopy. A theoretical model developed for the interaction of intense femtosecond laser pulses with solid targets on the basis of the two-temperature equation of state for an irradiated substance allows the description of the dynamics of the formation and scattering of the plasma. Comparison of the experimental data with the simulation results provides new information on the transport coefficients and absorption capacity of the nonideal plasma.

PACS numbers: 52.25.Os, 52.38.-r, 52.50.-b

DOI: 10.1134/S0021364007060021

The properties of a laser plasma formed on the surface of an aluminum target subjected to femtosecond laser pulses with power fluxes $\leq 10^{14}$ W/cm² have been investigated both experimentally and theoretically. Such laser pulses produce a thin layer of the nonideal solid plasma with an electron temperature up to ~ 10 eV. In contrast to works [1, 2], particular attention is focused on the initial stage (in the range 10^2 – 10^3 fs) of the heating and scattering of the plasma under the conditions of the undeveloped hydrodynamic motion of ions.

The investigations are performed using optical interferometric microscopy with femtosecond time resolution, which makes it possible to acquire information on the dynamics of change not only in the amplitude, but also in the phase of the reflected wave of probe radiation in the interaction region. Comparison of the numerical simulation results with the experimental data obtained makes it possible to determine the coefficients in the expressions for the effective electron collision frequency, in contrast to the models discussed in [2–4]. In contrast to the approach proposed in [5], this study is free of the assumptions that the metal is not melted and the electron temperature is much lower than the Fermi energy. This allows us to use the proposed model in a wide region of the parameters of the nonideal plasma formed on the target surface.

The source of radiation is a Cr:forsterite laser system generating femtosecond pulses at a wavelength of $\lambda_1 = 1240$ nm [6]. The FWHM of the pulses that is measured using an autocorrelator of the noncollinear second harmonic is equal to $\tau_L \approx 110$ fs in this experiment

for the sech² envelop shape. The time profile of the pulse is measured in a wide power range using the third-harmonic correlator. The ratio (contrast) of the intensity at the pulse maximum to the intensity 1 and 2 ps before the maximum is no less than 10^4 and 10^6 , respectively [7].

Figure 1 shows the measurement scheme based on a Michelson interferometer with the transfer of an image of the surface of the sample under investigation to the plane of the CCD matrix. Aluminum films ~ 1 μ m in thickness deposited on a glass substrate are used in the

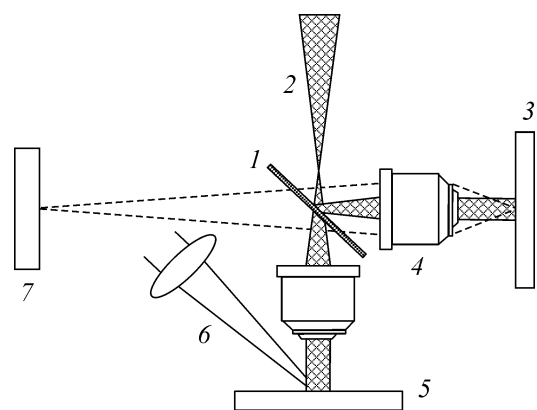


Fig. 1. Optical measurement scheme: (1) the beam splitter plate, (2) the probe pulse, (3) the reference mirror, (4) the microobjectives, (5) the target, (6) the heating pulse, and (7) the CCD matrix.

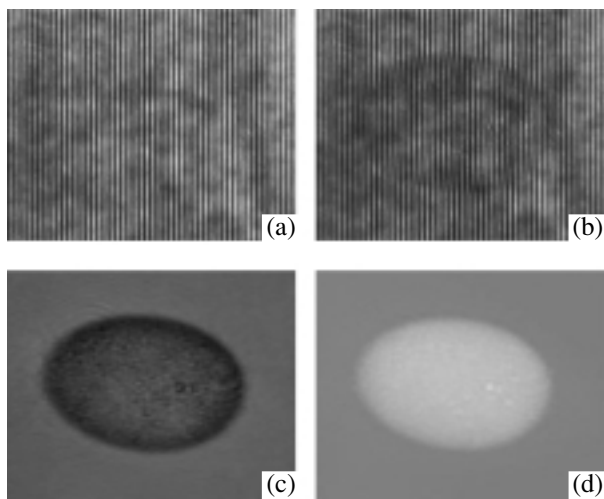


Fig. 2. Interference patterns of the aluminum target surface (a) before the action and (b) 530 fs after the action of the heating pulse and the reconstructed distributions of (c) r_{ind} and (d) Ψ_{ind} .

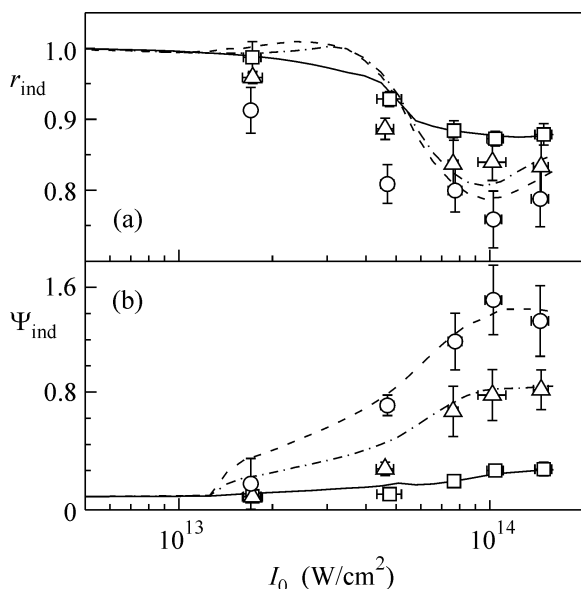


Fig. 3. Experimental points and calculated curves for (a) r_{ind} and (b) Ψ_{ind} vs. the intensity I_0 of the heating laser pulse for delay times $\Delta t = (\square$ and solid line) 130, $(\Delta$ and dash-dotted line) 530, and $(\circ$ and dashed line) 930 fs.

experiments. After each irradiation by the heating pulse, target is shifted to a new place.

The target is heated by a p polarized laser pulse at the main laser wavelength λ_1 for the angle of incidence 45° . The spatial distribution of the pumping radiation intensity on the target corresponds to the Gaussian with a focus beam diameter of about $70 \mu\text{m}$ at a level of e^{-2} . The probe pulse with varying time delay (the second

harmonic $\lambda_2 = 620 \text{ nm}$) is incident perpendicularly to the sample surface. The image of the surface of the sample under investigation is transferred to the CCD matrix plane by means of a microobjective with a numerical aperture of $N_A = 0.2$. The second reference arm of the interferometer includes a similar objective and a dielectric mirror with the wavelength λ_2 . The thermal radiation of the plasma is cut by a narrowband interferometer light filter. A probe beam (object) reflected from the sample interferes with the reference beam and forms an interference ring fringe in the CCD matrix plane.

A frame detected by the CCD matrix is a spatial intensity distribution $I(x, y) = |E_{\text{obj}}|^2 + |E_{\text{ref}}|^2 + 2\text{Re}\{E_{\text{obj}}E_{\text{ref}}^*\}$ as a result of the interference of the object $E_{\text{obj}}(x, y) = \tilde{r}(x, y)A_1(x, y)\exp[i\phi_1(x, y)]$ and reference $E_{\text{ref}}(x, y) = A_2(x, y)\exp[i\phi_2(x, y)]$ waves, where A_i and ϕ_i are the amplitudes and phases of interfering waves, respectively. In this case, the object wave carries information on the complex reflection coefficient of the sample, which can be represented in the form $\tilde{r}(x, y) = r(x, y)\exp[i\Psi(x, y)]$, where r and Ψ are the absolute value and phase of the complex reflection coefficient, respectively.

When processing the interference patterns by the Fourier transform algorithm [8, 9], laser-induced changes in r and Ψ are determined: $r_{\text{ind}}(x, y) = r_i(x, y)/r_i(x, y)$ and $\Psi_{\text{ind}}(x, y) = \Psi_i(x, y) - \Psi_i(x, y)$. Here, r_i (Ψ_i) and r_i (Ψ_i) are the absolute values (phases) of the complex reflection coefficients of the target before the action of the heating laser pulse and of the irradiated target, respectively.

The use of the CCD camera with 1024×1024 pixel matrix with a capacity of 12 bits allows us to perform measurements with an error of no more than 1% for change in the absolute value of the reflection coefficient and an error of $\sim\pi/200$ for change in the phase at a spatial resolution of $\sim 2 \mu\text{m}$.

Figure 2 shows the reconstructed changes $r_{\text{ind}}(x, y)$ and $\Psi_{\text{ind}}(x, y)$ in the region of heating by a laser pulse with $I_0 \approx 1.5 \times 10^{14} \text{ W/cm}^2$.

Figure 3 shows r_{ind} and Ψ_{ind} as functions of the maximum intensity I_0 of a heating laser pulse for various delay times ($\Delta t = 130, 530,$ and 930 fs) of the probe pulse with respect to the heating pulse. Each experimental point is a result of averaging over 5–10 measurements.

The theoretical lines in Fig. 3 are obtained by simulating the heating of the target of the intense laser pulse, as well as the formation and scattering of the plasma, with the calculation of the amplitude and phase of the reflected field of the probe pulse at the double frequency.

The self-consistent theoretical model includes the system of electrodynamic equations for describing the

absorption and reflection of laser radiation, ionization kinetic equations, and one-fluid hydrodynamic equations including electron–ion relaxation and electron heat conduction [10, 11], as well as a new broadband two-temperature equation of state of the irradiated substance.

For process times under consideration, $t \lesssim 1$ ps, all typical sizes of inhomogeneities in the z direction perpendicular to the target surface do not exceed $1 \mu\text{m}$ and are much smaller than the inhomogeneity sizes along the target surface, which are determined by the size of the focusing spot and are equal to tens of microns. For this reason, to analyze the experimental data, we use the one-dimensional version of the model developed that takes into account changes in all quantities only in the z direction and the single velocity component V of the quasineutral scattering of the plasma in the z direction perpendicular to the target surface.

The hydrodynamics equations of continuity for the volume concentration of heavy particles (atoms and ions) n_a and change in the substance momentum for the velocity V are written in the standard form including thermal ionization in the model of the average ion charge Z [10], and the equations for the energies of electrons e^e and heavy particles e^i have the form

$$Zn_a[\partial_t + V\partial_z]e^e = -\partial_z q_T - Q_Z + Q_{IB} - e^e\Theta - P_e\partial_z V - Q^{ei}, \quad (1)$$

$$n_a[\partial_t + V\partial_z]e^i = -P_i\partial_z V + Q^{ei}. \quad (2)$$

Here, P_e and P_i are the pressures of electrons and heavy particles, respectively, determined by the equation of state of the substance; Θ and Q_Z are the total rate of the thermal ionization and power density spent on ionization, respectively, which are calculated using the model of the average ion charge, the Lotz formula for impact ionization, and the detailed balance principle [10, 11]; $Q^{ei} = \gamma^{ei}Zn_a(T_e - T_i)$ is the electron–ion relaxation energy density, where T_e and T_i are the temperatures of electrons and heavy particles, respectively, and the coefficient γ^{ei} for lattice temperatures $T_i \lesssim T_{\text{melt}}$ (T_{melt} is the melting temperature) is a constant ($\gamma^{ei} = 4.93 \times 10^{10} \text{ s}^{-1}$ for aluminum) and, for higher temperatures, is determined by the plasma formula $\gamma^{ei} = 3(m_e/m_i)v_{\text{eff}}$, where m_e and m_i are the masses of the electron and heavy particle, respectively, v_{eff} is the effective electron collision frequency; $q_T = K'T_e\partial_z T_e$ is the electron thermal flux, where the coefficient K' for lattice temperatures $T_i \lesssim T_{\text{melt}}$ is a constant ($K' = 4.35 \times 10^{36} \text{ [erg cm s]}^{-1}$ for aluminum) and, for higher temperatures, is determined by the plasma formula $K' = -128\kappa_Z Zn_a/3\pi m_e v_{\text{eff}}$ [12] (the factor $\kappa_Z \approx 0.7$ presents the effect of electron–electron collisions on heat conduction); and $Q_{IB} = (8\pi)^{-1}\omega_1 \text{Im}\epsilon|\mathbf{E}|^2$ is the power density of the inverse bremsstrahlung absorption of the energy of the heating

laser pulse, where E is the electric-field amplitude in the laser pulse, ϵ is the dielectric constant, and ω_1 is the heating radiation frequency.

The amplitude of the strength vector of the p polarized electric field of the heating laser pulse is expressed in terms of the magnetic field strength for which the time-reduced wave equation [13] is solved numerically. The complex reflection coefficient of a weak s -polarized probe laser pulse is determined in the linear approximation. To this end, on the spatially inhomogeneous profile of the dielectric constant obtained for various delay times by solving the dynamic problem for the target irradiated by the heating laser pulse, the time reduced wave equation for the single electric field component of the probe pulse is solved numerically [13].

The effective collision frequency v_{eff} over the entire temperature range is determined as the minimum of the three values: $v_{\text{eff}} = \min\{v_{\text{met}}, v_{\text{pl}}, v_{\text{max}}\}$, where v_{met} is the effective collision frequency in the metal plasma for $T_e \lesssim$

$T_F = (3\pi^2 Zn_a)^{2/3} \hbar^2 / (2m_e)$, $v_{\text{pl}} = (4/3) \sqrt{2\pi} Z^2 n_a e^4 \Lambda / \sqrt{m_e T_e^3}$ is the collision frequency for the weakly nonideal plasma [14], Λ is the Coulomb logarithm, v_{max} is the maximum collision frequency determined by the condition that the collision mean free path of electrons, $\lambda_e \sim v_e/v_{\text{eff}}$ (v_e is the mean electron velocity) is no less than the mean distance between ions $r_0 \sim n_a^{-1/3}$ [15]:

$$v_{\text{max}} = k_1 \omega_{pe}, \quad (3)$$

$\omega_{pe} = \sqrt{4\pi n e^2 / m_e}$ is the electron plasma frequency and the numerical coefficient $k_1 \lesssim 1$ is chosen by fitting the calculations to the experimental data. Despite the simplicity of such approach to the determination v_{eff} , it ensures satisfactory accuracy as compared to much more complicated methods [16].

The effective collision frequency in the metal plasma v_{met} is determined as

$$v_{\text{met}} = C_{e-ph} T_i / \hbar + k_2 T_e^2 / \hbar T_F, \quad (4)$$

$$C_{e-ph} = C_{00} + C_0 [1 - \min\{T_i/T_{\text{melt}}, 1\}]^{1/2}. \quad (5)$$

The first and second terms in Eq. (4) present the contributions from the electron–phonon [17] and electron–electron [18] collisions, respectively. The constant k_2 is chosen by comparing with the experimental data (see also [5]). The first and second terms in Eq. (5) present the contributions from the intraband and interband transitions [17, 19], respectively. The constant C_{00} is determined from the data on the static conductivity of metals [19] (for aluminum $C_{00} \approx 3.28$). The constant C_0 is chosen so as to ensure the tabulated reflection coefficient $|r|^2$ of the metal under consideration at room temperature. For aluminum $|r|^2 \approx 0.96$ and 0.91 , whereas $C_0 \approx 23$ and 10 , for the heating pulse wavelengths $\lambda_1 = 1.24 \mu\text{m}$ and $\lambda_2 = 0.62 \mu\text{m}$, respectively. When the lat-

tice temperature T_i exceeds the melting temperature T_{melt} , the band structure of the metal is destroyed and the contribution from the interband transitions to the electron–phonon collision frequency vanishes [20]. This circumstance is taken into account by a phenomenological dependence on T_i/T_{melt} in Eq. (5).

The dielectric constant of the substance is determined by the Drude formula for the metallic plasma [19] for $T_e \leq T_1 = 0.75T_F$ and by the formula for a weakly nonideal nondegenerate plasma [10, 11, 14] for $T_e \geq T_2 = 1.5T_F$. In the interval $T_1 < T_e < T_2$, a linear interpolation between the Drude formula and plasma formula is used with the above-indicated v_{pl} value. The optical electron mass in the Drude formula is taken as $m_{\text{opt}} = 1.5m_e$ [20].

The thermodynamic characteristics of the condensed phase of the target substance for both thermal equilibrium between ions and electrons and nonequilibrium heating (when $T_e > T_i$) are determined by using a new semiempirical equation of state in a wide region of densities and temperatures. In this equation of state, the free energy $F(\rho, T_i, T_e, Z)$ is represented as the sum of two terms $F = F_i(\rho, T_i) + F_e(\rho, T_i, Z)$ determining the contributions of heavy particles and electrons, respectively ($\rho = m_i n_a$ is the substance density).

The first term $F_i = F_c(\rho) + F_a(\rho, T_i)$ includes the energy of the interaction between heavy particles and electrons at $T_i = T_e = 0$ (F_c) and contribution from the thermal motion of heavy particles (F_a). The dependence of cold energy $F_c(\rho)$ is determined by the procedure described in [21], which ensures the equality of the total pressure in the system to atmospheric pressure at normal density (for aluminum, $\rho_0 = 2.71 \text{ g/cm}^3$) and room temperature, as well as the agreement with the existing data of the impact experiments and Thomas–Fermi calculations with quantum and exchange corrections for the high energy densities. The thermal contribution of heavy particles to the free energy is given by the expression [22]

$$F_a(\rho, T_i) = \frac{3T_i}{2m_i} \ln \left(\frac{\Theta_a^2}{T_i^2} + \frac{T_a \sigma^{2/3}}{T_i} \right), \quad (6)$$

where $\sigma = \rho/\rho_0$. To determine the dependence of the typical temperature $\Theta_a = \Theta_a(\rho)$, we use the interpolation formula [23]

$$\Theta_a(\rho) = \sigma^{2/3} \exp \left[(\gamma_{0a} - 2/3) \frac{B_a^2 + D_a^2}{B_a} \right] \times \arctan \left(\frac{B_a \ln \sigma}{B_a^2 + D_a (\ln \sigma + D_a)} \right),$$

where γ_{0a} is the Grüneisen coefficient under normal conditions. The constants T_a , B_a , and D_a are determined from the requirement of the optimal description of the experimental data on the thermal expansion and impact compressibility of porous substance samples.

The free energy of the electron gas in the metal is given by the expression

$$F_e(\rho, T_e, Z) = -\frac{3Z}{2m_i} T_e \ln \left(1 + \frac{\pi^2 T_e}{6 T_F} \right). \quad (7)$$

Equation (7) for low and high temperatures is an equation for an ideal degenerate Fermi gas and an ideal Boltzmann gas of free electrons, respectively [24]. Expressions similar to Eq. (7) were previously used in the equations of state in [23, 25]. The internal energies of one heavy particle and electron, as well as the total pressures for heavy particles and electrons, are expressed in terms of F as $e^i = m_i [F_i - T_i (\partial F_i / \partial T_i)_\rho]$ and $e^e = m_i Z^{-1} [F_e - T_e (\partial F_e / \partial T_e)_{\rho, Z}]$, as well as $P_i = \rho^2 (\partial F_i / \partial \rho)_{T_i}$ and $P_e = \rho^2 (\partial F_e / \partial \rho)_{T_e, Z}$, respectively.

Comparison of the experimental data with the calculations of the absolute value r_{ind} and phase Ψ_{ind} of the complex reflection coefficient of the probe pulse (see Fig. 3) makes it possible to determine (in the framework of this model) the important properties of the nonideal solid plasma such as the maximum effective frequency of electron momentum relaxation given by Eq. (3) and the contribution to the effective electron–electron collision frequency specified by Eq. (4). The best agreement with the experimental data for the aluminum targets is reached at $k_1 \approx 0.3$, which is close to the theoretical estimate [15] and at $k_2 \approx 0.85$ in Eqs. (3) and (4) for the effective collision frequencies. In this case, uncertainty in the choice of the coefficients does not exceed 15% including the experimental errors.

For the indicated parameters, the proposed model well reproduces r_{ind} and phase Ψ_{ind} as functions of the laser pumping pulse intensity I_0 for all time delays Δt between the pumping pulse and probe pulse in the measurements with $I_0 \geq 5 \times 10^{13} \text{ W/cm}^2$. For fluxes $I_0 \leq 5 \times 10^{13} \text{ W/cm}^2$, the model is in agreement with the experimental data for $\Delta t < 500 \text{ fs}$, whereas significant discrepancies exist for r_{ind} for $\Delta t > 500 \text{ fs}$. These discrepancies can be caused by the formation of a two-component mixture consisting of the low-density plasma and condensed-phase fragments on the target surface [26]. A detailed description of this effect is beyond the scope of the model and is the subject of further investigations.

Figure 4 shows the electron and ion temperatures, the substance density, the effective collision frequency, and the field strength of the laser probe pulse, as well as the nonideality parameter $\Gamma_{ei} = Ze^2 / (n_a^{-1/3} T_e)$ and the degeneration parameter $n\lambda_e^3 = (8\pi/3)(T_F/T_e)^{3/2}$, as func-

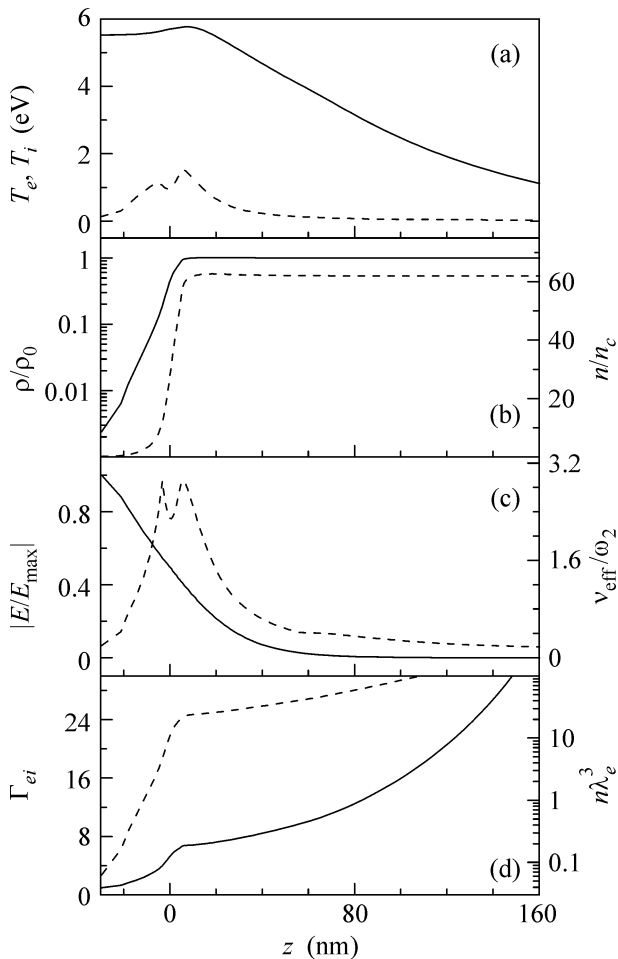


Fig. 4. Target-depth dependences calculated for the aluminum plasma parameters for $\Delta t = 530$ fs and $I_0 = 6.7 \times 10^{13}$ W/cm²: (a) temperatures of (solid line) electrons and (dashed line) ions; (b) normalized (solid line) density and (dashed line) electron concentration $n_c = m_e \omega_2^2 / 4\pi e^2$, where ω_2 is the frequency of the probe laser pulse; (c) normalized (solid line) electric field strength of the probe pulse and (dashed line) effective frequency of electron collisions; and (d) the parameters of (solid line) nonideality and (dashed line) degeneration.

tions of the target depth for the fixed intensity $I_0 = 6.7 \times 10^{13}$ W/cm² and the delay time $\Delta t = 530$ fs. Note that the average ion charge for the parameters under consideration does not change in the calculation time and remains equal to its initial value $Z = 3$.

As seen in Fig. 4, the plasma parameters are strongly inhomogeneous in the skin-layer region, where the reflected-signal field of the laser probe pulse is formed. For this reason, despite short durations of the processes under consideration, the Fresnel formulas describing the reflection from a *homogeneous* medium with a stepwise boundary are inapplicable to the calculation of the reflection coefficient and its phase.

Analysis of simulation results shown in Fig. 4 indicates that the electron temperature in the plasma formed on the target surface for the experimental parameters under consideration is much higher than the ion temperature and the plasma is in a strongly nonideal state (nonideality parameter $\Gamma_{ei} > 1$) and is strongly degenerate in the entire region except for the plasma corona.

In conclusion, we emphasize that the dependences of the amplitude and phase of the reflected field of the short laser probe pulse on its delay time and heating pulse intensity that are obtained by means of the experimental procedure used in this work make it possible to acquire important information on the transfer properties of the strongly nonideal plasma formed under the action of laser radiation on the target surface in the subpicosecond time intervals. It is shown that the plasma inhomogeneity decisively affects the reflective properties of the target even in such short times.

This work was supported in part by the Russian Foundation for Basic Research (project nos. 04-02-17055 and 06-02-17464) and the Council of the President of the Russian Federation for Support of Young Russian Scientists and Leading Scientific Schools (project no. NSH-3683.2006.2).

REFERENCES

1. A. R. Rundquist, J.-S. Lee, and M. C. Downer, *Phys. Rev. Lett.* **82**, 4010 (1999).
2. V. D. Urlin and B. P. Yakutov, *Kvantovaya Élektron. (Moscow)* **30**, 889 (2000).
3. K. Eidmann, J. Meyer-ter-Vehn, T. Schlegel, and S. Huller, *Phys. Rev. E* **62**, 1202 (2000).
4. J. P. Colombier, P. Combis, F. Bonneau, et al., *Phys. Rev. B* **71**, 165406 (2005).
5. V. A. Isakov, A. P. Kanavin, and S. A. Uryupin, *Kvantovaya Élektron. (Moscow)* **36**, 928 (2006).
6. M. B. Agranat, S. I. Ashitkov, A. A. Ivanov, et al., *Kvantovaya Élektron. (Moscow)* **34**, 506 (2004).
7. M. B. Agranat, N. E. Andreev, S. I. Ashitkov, et al., *Pis'ma Zh. Éksp. Teor. Fiz.* **83**, 80 (2006) [*JETP Lett.* **83**, 72 (2006)].
8. M. Takeda, H. Ina, and S. Kobayashi, *J. Opt. Soc. Am.* **72**, 156 (1982).
9. V. V. Temnov, K. Sokolowski-Tinten, P. Zhou, and D. von der Linde, *J. Opt. Soc. Am. B* **23**, 1954 (2006).
10. N. E. Andreev, M. E. Veisman, V. P. Efremov, and V. E. Fortov, *Teplofiz. Vys. Temp.* **41**, 679 (2003) [*High Temp.* **41**, 594 (2003)].
11. M. Veysman, B. Cros, N. E. Andreev, and G. Maynard, *Phys. Plasmas* **13**, 053114 (2006).
12. L. Spitzer and R. Harm, *Phys. Rev.* **89**, 977 (1953).
13. V. L. Ginzburg, *The Propagation of Electromagnetic Waves in Plasmas*, 2nd ed. (Nauka, Moscow, 1967; Pergamon, Oxford, 1970).
14. V. P. Silin and A. A. Rukhadze, *Electromagnetic Properties of Plasma and Plasma-like Media* (Atomizdat, Moscow, 1961) [in Russian].

15. I. T. Yakubov, Usp. Fiz. Nauk **163** (5), 35 (1993) [Phys. Usp. **36**, 365 (1993)].
16. D. Semkat, R. Redmer, and Th. Bornath, Phys. Rev. E **73**, 066406 (2006).
17. D. Fisher, M. Fraenkel, Z. Henis, et al., Phys. Rev. E **65**, 016409 (2001).
18. A. A. Abrikosov, *Fundamentals of the Theory of Metals* (Nauka, Moscow, 1987; North-Holland, Amsterdam, 1988).
19. N. W. Ashcroft and N. D. Mermin, *Solid State Physics* (Holt, Rinehart, and Winston, New York, 1976; Mir, Moscow, 1979), Vol. 1.
20. E. D. Palik, *Handbook of Optical Constants of Solids* (Academic, London, 1985).
21. K. V. Khishchenko, Pis'ma Zh. Tekh. Fiz. **30** (19), 65 (2004) [Tech. Phys. Lett. **30**, 829 (2004)].
22. A. V. Bushman, I. V. Lomonosov, and V. E. Fortov, *Equations of State of Metals at High Energy Densities* (Inst. Khim. Fiz. Ross. Akad. Nauk, Chernogolovka, 1992) [in Russian].
23. L. V. Al'tshuler, A. V. Bushman, M. V. Zhernokletov, et al., Zh. Éksp. Teor. Fiz. **78**, 741 (1980) [Sov. Phys. JETP **51**, 373 (1980)].
24. L. D. Landau and E. M. Lifshitz, *Course of Theoretical Physics, Vol. 5: Statistical Physics*, 4th ed. (Nauka, Moscow, 1995; Butterworth, London, 1999), Part 1.
25. M. M. Basko, Teplofiz. Vys. Temp. **23**, 483 (1985).
26. M. E. Povarnitsyn, T. E. Itina, P. R. Levashov, and K. V. Khishchenko, *Physics of Extreme States of Matter—2007* (Inst. Probl. Khim. Fiz. Ross. Akad. Nauk, Chernogolovka, 2007), p. 16 [in Russian].

Translated by R. Tyapaev

SPELL: OK